Supporting Information

Facile construction of $MgCo_2O_4$@$NiMoO_4$/NF core-shell nanocomposite for high-performance asymmetric supercapacitor

Haiwen Gao, Xiaohong Wang*, Ganghu Wang,, Chen Hao*, Chengxiang Huang and Chenglong Jiang

School of Chemistry and Chemical Engineering, Jiangsu University, Zhenjiang, Jiangsu 212013, China

*Corresponding author. Tel.: +86 511 88791800; fax: +86 511 88791800.

E-mail addresses: xhwang@ujs.edu.cn (X.H. Wang); chhao@ujs.edu.cn (C. Hao).

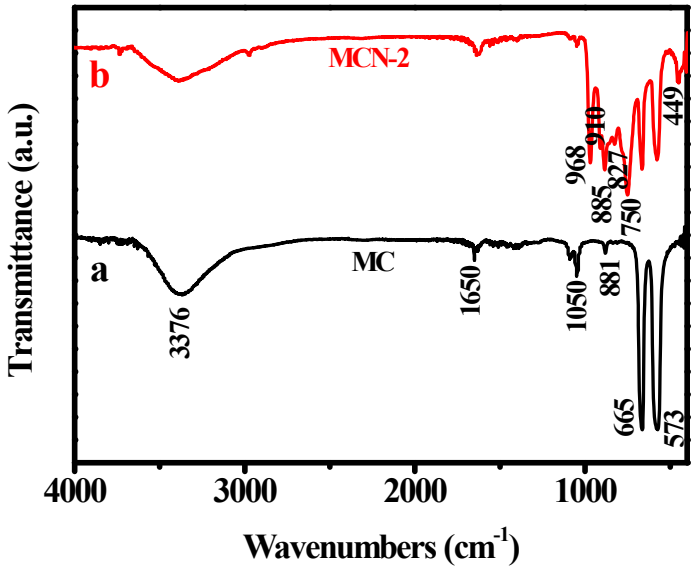

Fig. S1. FTIR spectra of the (a) MC, (b) MCN-2 electrode materials.

In order to study the structure and chemical bond of the product, characterize and identify the chemical species, FTIR test is carried out on our products. Fig. S1 shows the FTIR spectra of MC and MCN-2 electrode materials in the range of 400-4000 cm^{-1}. It can be seen that the FTIR spectrum of MC electrode material has six absorption peaks at 573 cm^{-1}, 665 cm^{-1}, 881 cm^{-1}, 1050 cm^{-1}, 1650 cm^{-1} and 3376 cm^{-1}, as shown in Fig. S1a. Thereinto, the characteristic bands of MC material at 573 cm^{-1}, 665 cm^{-1}, 881 cm^{-1} and 1050 cm^{-1} correspond to Mg-O stretching vibration, Mg-O-Mg bending vibration, Co-O-Co bending vibration and Co-O stretching vibration bonds, respectively [1,2]. Typically, the characteristic peak at 1650 cm^{-1} is assigned to variable angle vibration of liquid H_2O. The broad absorption peak at 3376 cm^{-1} is attributed to the stretching vibration of hydroxyl peak [3]. In addition, the peak of MCN-2 electrode material at 449 cm^{-1} is due to a superposition of v_4 and v_5 of MoO_3 and v_3 of NiO groups in the $NiMoO_4$ [4,5]. The bands at 827 cm^{-1} and 885 cm^{-1} correspond to the stretching vibration of Mo-O-Mo [6]. Simultaneously, the absorption peaks at 750 cm^{-1}, 910 cm^{-1} and 968 cm^{-1} are assigned to the v_3 vibration and stretching vibration of Mo=O [7].

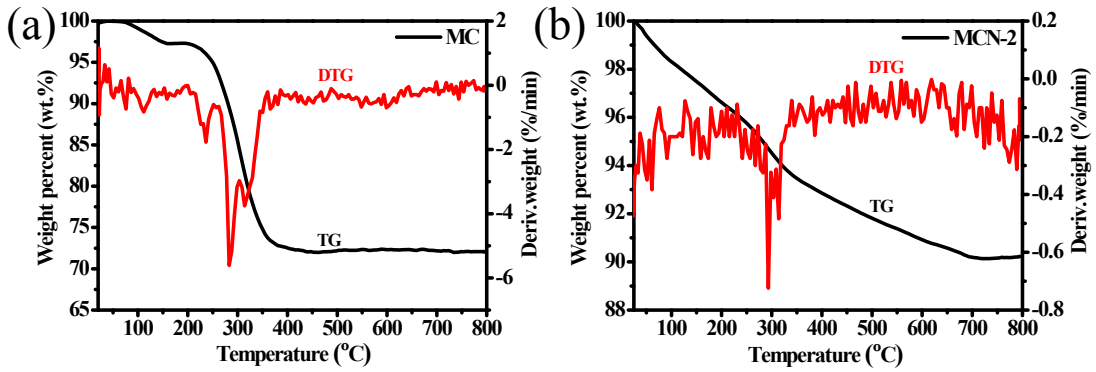

Fig. S2. TGA and DTG curves of double urchin-like hierarchical (a) MC, (b) MCN-2 electrode materials.

The TGA and DTG measurements of MC and MCN-2 electrode materials are carried out to study the thermal stability and components of the materials, as shown in Fig. S2. The condition of the tests are a temperature range (from room temperature to 800 ℃) and a temperature rate (10 ℃ min^{-1}). Obviously, there are two stages of weight loss for MC electrode material, as shown in Fig. S2a. The first stage reduces 2.7 % of the original weight at 200℃, which is due to the loss of surface water and crystal water for the sample. Moreover, the second stage reduces 24.8 % of the original weight at 400℃, which is attributed to oxidation decomposition of metal salts. At this stage, the fastest point of degradation occurs at 283℃ according to the DTG curve, and the point has important implications for the formation of the crystalline form. The TGA and DTG measurements of MCN-2 electrode material is performed for comparison. As depicted in Fig. S2b, it also has two stages for MCN-2 electrode material. The first stage reduces 1.6 % of the original weight at 91 ℃, which is attributed to the loss of surface water and crystal water for the sample. In addition, the second stage reduces 8.2 % of the original weight at 700℃, which is attributed to oxidation decomposition of metal salts. The comparison between the two shows that MCN-2 has better thermal stability.

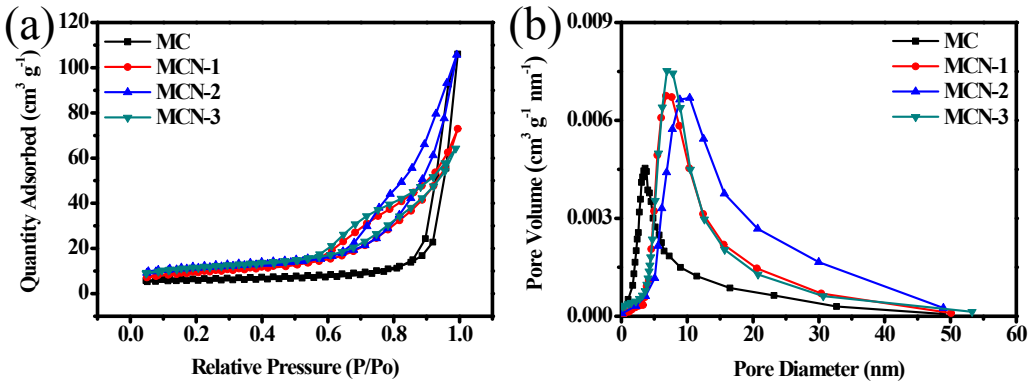

Fig. S3. (a) N_2 adsorption-desorption isotherms and (b) pore size distributions of MC, MCN-1, MCN-2 and MCN-3.

The adsorption-desorption isotherms and pore size distributions of MC, MCN-1, MCN-2 and MCN-3 are shown in Fig. S3. The specific surface area of MC, MCN-1, MCN-2 and MCN-3 is calculated to be 25.5, 33.6, 40.1 and 39.3 m^2 g^{-1}, respectively. Obviously, the isotherms of all active materials are IV-type isotherms. In addition, the pore size distributions of MC, MCN-1, MCN-2 and MCN-3 are about 3.5, 7, 9.7 and 7.2 nm, respectively. The above results prove that MCN-2 has a large specific surface area, which can provide more active sites for chemical reactions and meet the needs of electron transfer and ion transmission.

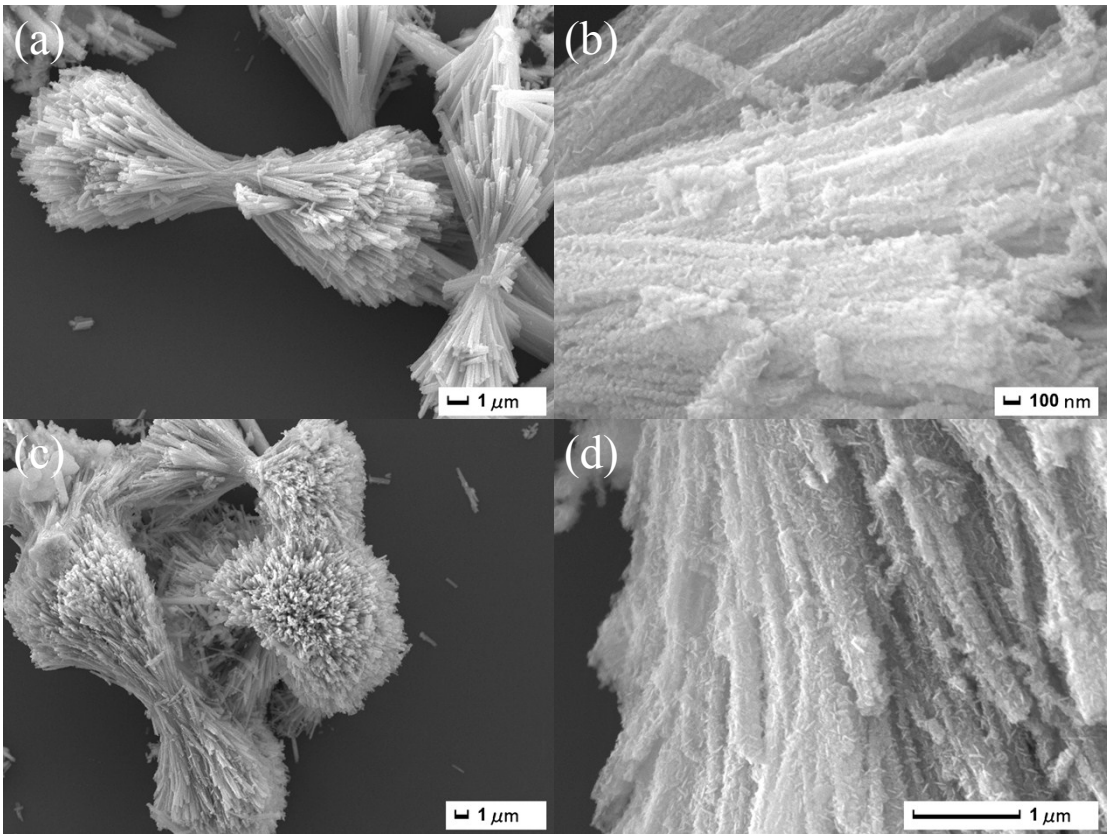

Fig. S4. FE-SEM images of MCN-1 at low (a) and high (b) magnification. FE-SEM images of MCN-3 at low (c) and high (d) magnification.

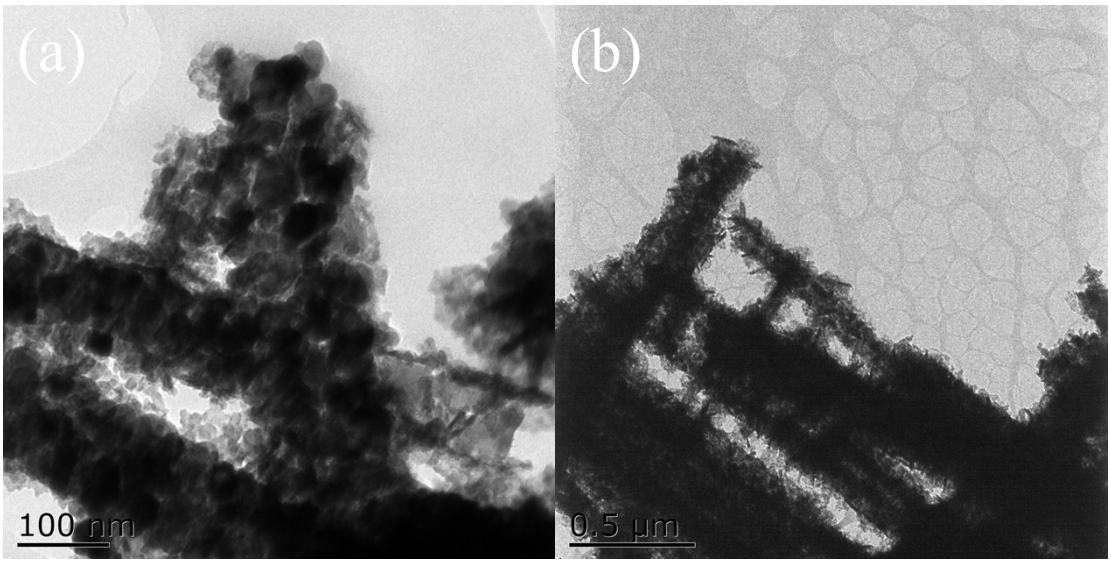

Fig. S5. TEM images of (a) MCN-1 and (b) MCN-3 electrode materials.

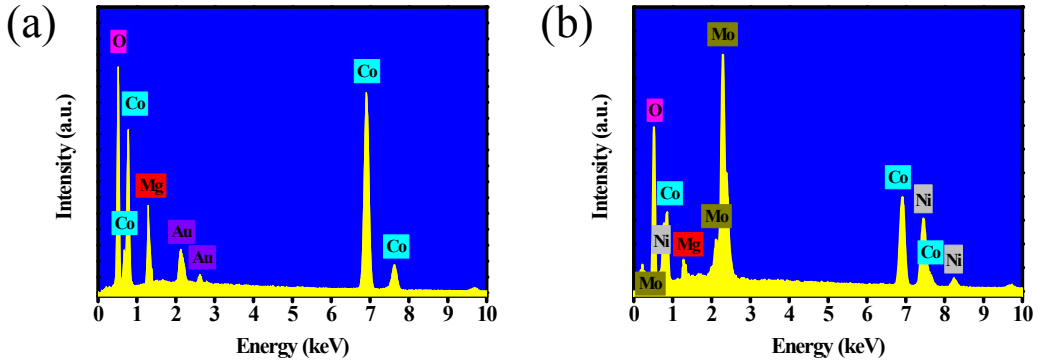

Fig. S6. EDX spectrums for double urchin-like hierarchical (a) MC and (b) MCN-2 electrode materials.

The elemental composition of MC and MCN-2 electrode materials is studied through EDX spectrums, as shown in Fig. S6. It can be seen that the MC electrode material has only four elements (O, Co, Mg and Au). The Au is the conductive material, which is sprayed on the surface of the electrode material to make the conductive performance of electrode material better. In addition, the MCN-2 electrode material has six elements (O, Co, Mg, Au, Ni and Mo), as shown in Fig. S6b.

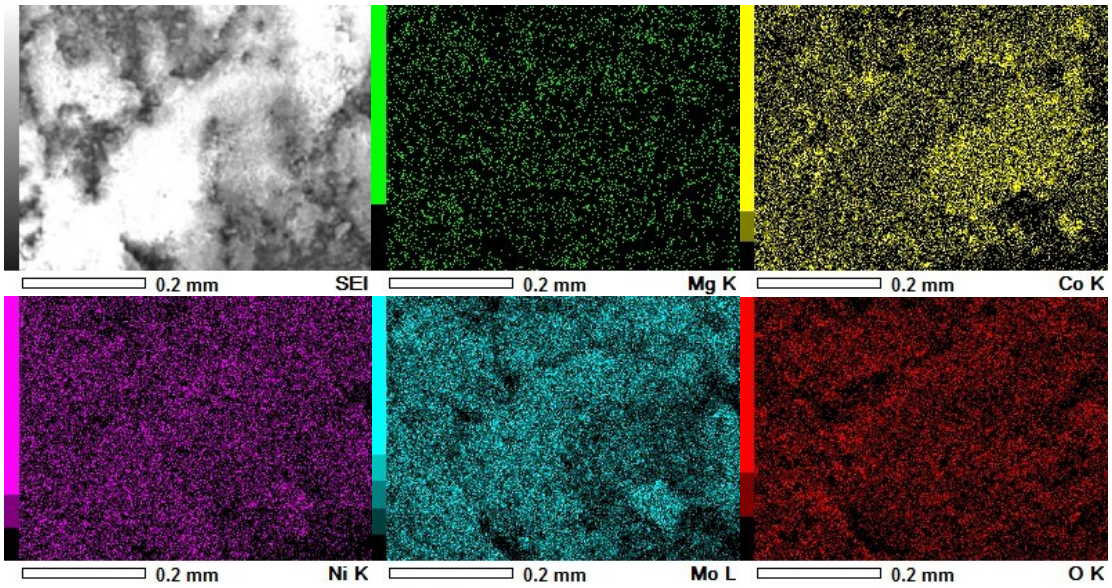

Fig. S7. Mapping of double urchin-like hierarchical MCN-2 electrode material.

As shown in Fig. S7, it can be seen that the MCN-2 electrode material has the Mg, Co, Ni, Mo and O elements, without any other ones. The mapping of double urchin-like hierarchical MCN-2 electrode material indicates that the result is consistent with EDX spectrums for double urchin-like hierarchical MCN-2.

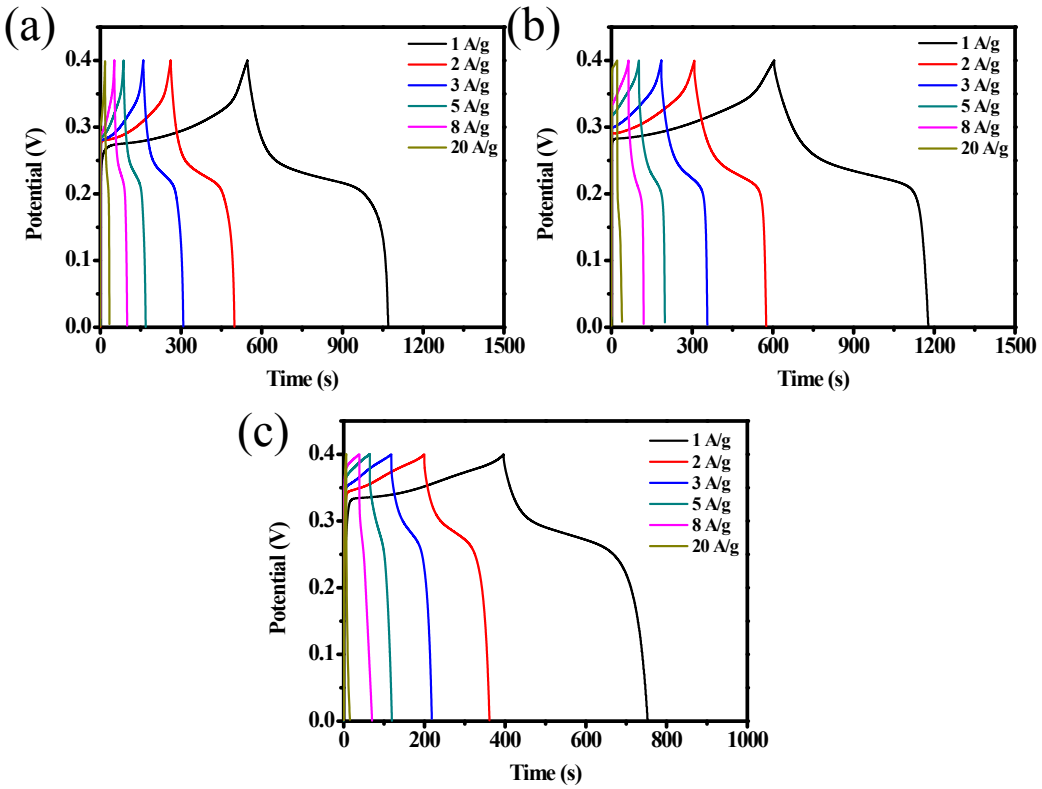

Fig. S8. (a) GCD curves of MCN-1 electrode material at different current densities. (b) GCD curves of MCN-3 electrode material at different current densities. (c) GCD curves of NM electrode material at different current densities.

Fig. S8 shows the GCD curves of MCN-1, MCN-3 and NM electrode materials at the current densities of 1, 2, 3, 5, 8 and 20 A g^{-1}. The specific capacitances of MCN-1, MCN-3 and NM electrode materials are 1307.5, 1432.5, 892.6 (1 A g^{-1}) F g^{-1}; 1184.6, 1334.5, 807.3 (2 A g^{-1}) F g^{-1}; 1115.2, 1280.9, 752.5 (3 A g^{-1}) F g^{-1}; 1026.7, 1204.1, 685.8 (5 A g^{-1}) F g^{-1}; 956, 1130, 631.3 (8 A g^{-1}) F g^{-1}; 815.9, 902.5, 455.2 (20 A g^{-1}) F g^{-1}, respectively, which can be obtained by the formula of specific capacitance.

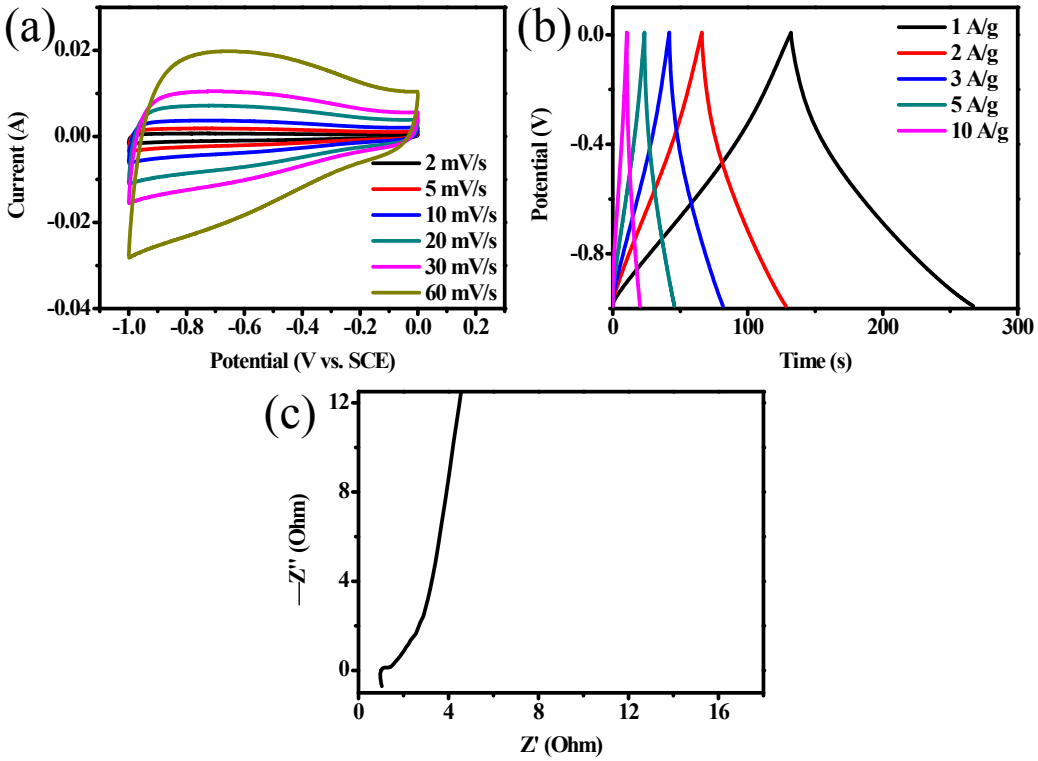

Fig. S9. (a) CV curves of AC at different scan rates. (d) GCD curves of AC at different current densities. (c) Nyquist impedance plot of AC.

Fig. 9a shows the CV curves of AC at different scan rates in the potential window from -1 to 0 V. It can be seen that the curves show evident quasi-rectangular shape, indicating that AC electrode has good reversible charge-discharge performance. Fig. S9b shows the GCD curves of AC at the current densities of 1-20 A g^{-1}. It can be seen that the specific capacitances are 135, 124.5, 119.4, 111 and 97.2 F g^{-1}, respectively. In addition, the AC electrode has a lower resistance, as shown in Fig. S9c.

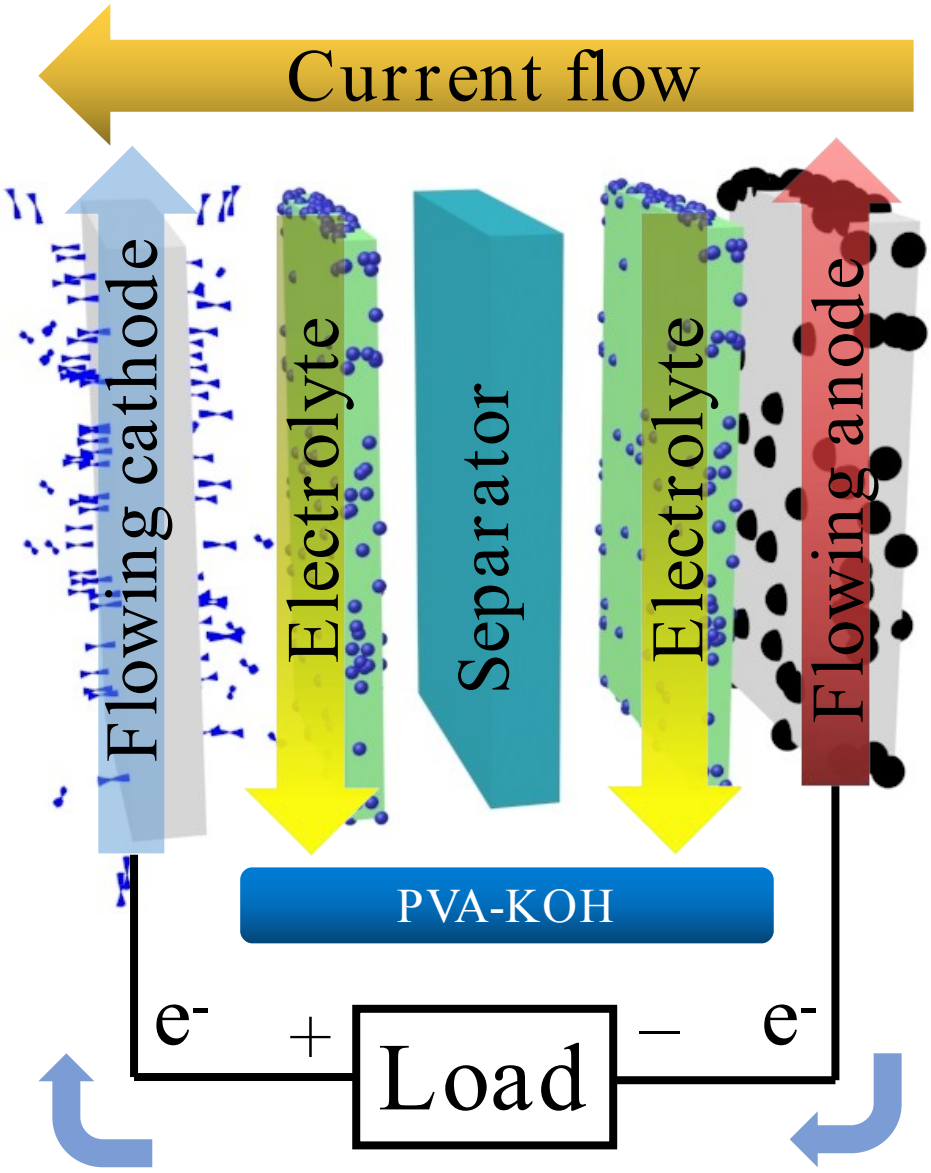

Fig. S10. Configuration diagram for ASC device.

The practical application of electrode material is very important. Therefore, we have assembled all-solid-state asymmetric supercapacitor using the electrode material (MCN-2), as shown in Fig. S10. Among which, the AC electrode serves as a negative electrode, a cellulose diaphragm (preventing short circuit) as a separator and the PVA-KOH gel (providing ions for the reaction) as an electrolyte. Moreover, the mass of cathode and anode materials is obtained by the balance formula of charge:

$$Q = C_s \Delta V m \quad (1)$$

$$\frac{m_+}{m_-} = \frac{C_{s-} \Delta V_-}{C_{s+} \Delta V_+} \quad (2)$$

Where m_+ (g), Cs_+ (F g^{-1}), ΔV_+ (V), m_- (g), Cs_- (F g^{-1}) and ΔV_- (V) represent the mass (g) of the active material, the specific capacitance of the active material, the potential window of the active material, the mass (g) of the AC, the specific capacitance of the AC, the potential window of the AC, respectively. According to the above formula, the specific capacitance of MCN-2 (1775 F g^{-1}, 1 A g^{-1}) and the specific capacitance of AC (135 F g^{-1}, 1 A g^{-1}), the theoretical mass ratio of MCN-2 and AC is calculated as 0.19.

It is easy to find that AC electrode stores capacitance by adsorbing and desorbing surface charges, while MCN-2 electrode mainly stores capacitance by electrochemical reaction, so the capacitance of MCN-2 electrode is larger than that of AC electrode.

In addition, mass specific capacity (C_m) is an important parameter for supercapacitor. Since supercapacitors have properties similar to batteries, we can calculate the capacity performance of supercapacitors by the following formula:

$$C_m = 3.6 \times C_s \triangle V \quad (3)$$

Where C_s (105.4 F g^{-1}, 0.6 A g^{-1}) is the specific capacitance of MCN-2//AC ASC device and ΔV (1.6 V) represent the potential window of MCN-2//AC ASC device. According to the above formula, the C_m of MCN-2//AC ASC device is calculated as 607.1 mAh g^{-1}.

Fig. S11. A photograph of two MCN-2//AC ASCs in series.

Table S1. Comparison of the electrochemical properties of the similar materials previously reported and the present work.

Electrode materials	Specific (Areal) capacitance	Rate performance	Capacity retention	Reference
$MgCo_2O_4$ nanocone arrays	750 F/g (1 A/g)	59.4 % (20 A/g)	84 % (1000 cycles)	8
Double-urchin-like $MgCo_2O_4$	508 F/g (2 A/g)	29.9 % (40 A/g)	95.9 % (2000 cycles)	9
1D $MgCo_2O_4$	752 F/g (2 mA/cm^2)	12.6 % (30 mA/cm^2)	/	10
$MgCo_2O_4$ nanobrush/carbon fiber	854 mF/cm^2 (2.5 mA/cm^2)	93.5 % (20 mA/cm^2)	/	11
$MgCo_2O_4$ cuboidal microcrystals	690 F/g (1 A/g)	41.7 % (15 A/g)	110 % (3000 cycles)	12
$MgCo_2O_4$ SMPs	613.5 C/g (2 mA/cm^2)	34.4 % (40 mA/cm^2)	66.7 % (5000 cycles)	13
$MgCo_2O_4$ nanowires	658 F/g (1 A/g)	76 % (50 A/g)	85.6 % (2000 cycles)	14
$MgCo_2O_4$ nanosheets	947 C/g (2 A/g)	/	96 % (5000 cycles)	15

$MgCo_2O_4$@PPy	1079.6 F/g (1 A/g)	77 % (20 A/g)	97.4 % (1000 cycles)	16
$NiMoO_4$@PANI	1214 F/g (1 A/g)	67 % (20 A/g)	80.7 % (2000 cycles)	17
$CuCo_2O_4$@$NiMoO_4$	2207 F/g (1.25 A/g)	70.7 % (25 A/g)	95.6 % (5000 cycles)	18
$NiMoO_4$@Ni-Co-S-8	2.27 F/cm^2 (5 mA/cm^2)	44.5 % (40 mA/cm^2)	91.7 % (6000 cycles)	19
$MgCo_2O_4$@$NiMoO_4$	**1775 F/g (1 A/g)**	**67.1 % (20 A/g)**	**74.7 % (5000 cycles)**	**This work**

References

[1] M. L. Yan, Y. D. Yao, J. Q. Wen, L. Long, M. L. Kong, G. G. Zhang, X. M. Liao, G. F. Yin and Z. B. Huang, *ACS Appl. Mater. Interfaces*, 2016, **8**, 24525-24535.

[2] L. R. Hou, C. Z. Yuan, D. K. Li, L. Yang, L. F. Shen and F. Zhang, *Electrochim. Acta*, 2011, **56**, 7454-7459.

[3] Y. Meng, F. H. Su and Y. Z. Chen, *ACS Appl. Mater. Interfaces*, 2015, **7**, 11604-11612.

[4] M. Masteri-Farahani, S. Mahdavi and M. Rafizadeh, *Ceram. Int.*, 2013, **39**, 4619-4625.

[5] D. Klissurski, M. Mancheva, R. Iordanova, G. Tyuliev and B. Kunev, *J. Alloy. Compd.*, 2006, **422**, 53-57.

[6] G. Kianpour, M. Salavati-Niasari and H. Emadi, *Ultrason. Sonochem.*, 2013, **20**, 418-424.

[7] H. Oudghiri-Hassani and F. Al Wadaani, *Molecules*, 2018, **23**, 273.

[8] L. F. Cui, L. H. Huang, M. Ji, Y. G. Wang, H. C. Shi, Y. H. Zuo and S. F. Kang, *J. Power Sources*, 2016, **333**, 118-124.

[9] J. S. Xu, L. Wang, J. Zhang, J. H. Qian, J. Liu, Z. Q. Zhang, H. D. Zhang and X. Y. Liu, *J. Alloy. Compd.*, 2016, **688**, 933-938.

[10] M. Silambarasan, P. S. Ramesh, D. Geetha and V. Venkatachalam, *J. Mater. Sci.-Mater. Electron.*, 2017, **28**, 6880-6888.

[11] X. M. Wu, L. Meng, Q. G. Wang, W. Z. Zhang and Y. Wang, *Mater. Lett.*, 2017, **206**, 71-74.

[12] S. G. Krishnan, M. Harilal, I. I. Misnon, M. V. Reddy, S. Adams and R. Jose, *Ceram. Int.*, 2017, **43**, 12270-12279.

[13] H. Y. Gao, Y. F. Li, H. H. Zhao, J. J. Xiang and Y. Cao, *Electrochim. Acta*, 2018, **262**, 241-251.

[14] X. F. Guan, Q. R. Wang, P. H. Luo, Y. L. Yu, X. Y. Li, Y. Zhang and D. G. Chen, *Int. J. Electrochem. Sci.*, 2018, **13**, 2272-2285.

[15] S. Vijayakumar, S. Nagamuthu and K. S. Ryu, *Dalton Trans.*, 2018, **47**, 6722-6728.

[16] H. W. Gao, X. H. Wang, G. H. Wang, C. Hao, S. S. Zhou and C. X. Huang, *Nanoscale*, 2018, **10**, 10190-10202.

[17] H. W. Gao, F. S. Wu, X. H. Wang, C. Hao and C. W. Ge, *Int. J. Hydrog. Energy*, 2018, 43, 18349-18362.

[18] J. H. Lin, H. Y. Liang, H. N. Jia, S. L. Chen, Y. F. Cai, J. L. Qi, J. Cao, W. D. Fei and J. C. Feng, *Inorg. Chem. Front.*, 2017, **4**, 1575-1581.

[19] C. Chen, D. Yan, X. Luo, W. J. Gao, G. J. Huang, Z. W. Han, Y. Zeng and Z. H. Zhu, *ACS Appl. Mater. Interfaces*, 2018, **10**, 4662-4671.